INT. J. CONTROL, 2000, VOL. 73, NO. 6, 531–544

Model-free controller design for a single-link flexible smart materials robot

S. S. GE*†, T. H. LEE†, J. Q. GONG† and Z. P. WANG†

In this paper, controller design is investigated for a single-link flexible smart materials robot which combines the advantages of both flexible link robots and piezoelectric materials. To avoid the drawbacks resulting from model uncertainties and/or model truncations, model-free controllers (both decentralized and centralized) are proposed for tip regulation and residual vibration suppression. In contrast to traditional model-based methods, the controllers presented in the paper are derived from the basic energy–work relationship and can guarantee the asymptotic stability of the damped truncated system with arbitrarily any finite number of flexible modes. Furthermore, the controllers are easily implementable because all the signals can be chosen to be readily measurable. Simulations are carried out to show the effectiveness of the approach presented.

1. Introduction

In order to overcome the drawbacks related to rigid robots, such as heavy weight, low operational speed and large energy consumption, controller design for flexible robots has been intensively studied. The undesired residual vibrations of flexible robots are difficult to control with high precision. For a traditional flexible robot, there is only one motor for each link acting as an actuator. However, the flexible link robot is governed by a set of partial differential equations (PDEs), which means that the system is of infinite dimensionality. Consequently, complicated control techniques have to be used for better control precision (Siciliano and Book 1988, Lanari and Wen 1992, Shifman 1993, Aoustin *et al.* 1994, Ge *et al.* 1996, Zhu *et al.* 1997, Ge *et al.* 1998c). Singular perturbation techniques were applied to the control of flexible robots in Siciliano and Book (1988). In Lanari and Wen (1992), a family of asymptotically stabilizing control laws was introduced for a class of non-linear Hamilton systems and applied to flexible robots. Comparison studies between linear PD control, LQR control, feedback linearization control, singular perturbation method and sliding mode control were investigated in Aoustin *et al.* (1994) with respect to a single-link flexible robotic arm. Non-model-based controllers were investigated to avoid the drawbacks of truncated-model-based controller design (Ge *et al.* 1996, 1998c). A backstepping approach was applied to a simple lumped model for the flexible robot in Zhu *et al.* (1997). Tracking control of an Euler–Bernoulli beam was discussed in Shifman (1993) under the assumption that there is no tip payload and no motor hub inertia. As there are an infinite number of degrees of freedom to be controlled, yet only a finite number of actuators are available for control action, there is a limit to further improvment of control performance for conventional flexible link robots.

Since piezoelectric materials can be bonded or embedded along a beam and achieve the transformation between mechanical deformation and electrical field, they are ready to serve as actuators and sensors. Hence, an alternative approach to the control of flexible robots is the use of 'smart materials', i.e. materials embedded or bonded with a network of distributed actuators, sensors and processors. While such a robot retains all the advantages of a conventional flexible link robot, such as light weight and high operational speed, it has additional sensing and control capabilities. With the application of smart materials, better control performance for flexible robots is expected to be easily obtainable.

Much theoretical and experimental work has been carried out on both modelling and controller design of smart materials beams (Baily and Hubbard 1985, Crawley and Luis 1987, Varadan *et al.* 1990, Cundari and Abedian 1991, Yang and Lee 1994, Won 1995, Vukovich and Yousefi-Koma 1996). Surface-bonded and embedded piezoelectric actuators were modelled and analysed in Crawley and Luis (1987). An electromechanically coupled model of piezoelectric materials was given in Won (1995). In Bail and Hubbard (1985), by incorporating the piezoelectric moment in the static case, a model was derived on the basis of conventional Bernoulli–Euler beam theory and dynamic force balance, and a velocity feedback controller was investigated. Interactions between the host structures and the piezoelectric actuators were investigated experimentally by Yang and Lee (1994). From the viewpoint of virtual work, based on the model derived in Baily and Hubbard (1985), a series solution was obtained in Cundari and Abedian (1991). In Varadan *et al.* (1990), a cantilever beam with two segmented smart materials patches bonded on both sides near the fixed end was firstly

First received 5 January 1998. Revised 15 June 1999.

* Author for correspondence. e-mail: elegesz@nus.edu.sg

† Department of Electrical Engineering, National University of Singapore, Singapore 117576

modelled as a pure beam with its natural frequencies modified by experimental data, then constant gain, variable gain, bang-bang controllers were investigated experimentally on the basis of this model. In Vukovich and Yousefi-Koma (1996), a truncated wave model was developed and a wave-absorbing controller constructed, which is optimal in the sense of minimum output/input energy ratio. All these controllers were designed on the assumption that the system was exactly modelled. However, this assumption is too ideal to be true in practice. At the same time, there are unavoidable spillovers in the truncated models because a smart materials beam is described by PDEs, which means that the system is actually infinite dimensional.

In this paper, a single-link flexible robot with a finite number of segmented piezoelectric patches bonded along the link is discussed. For brevity, it is called a smart materials robot in this paper. This system is similar to that in Varadan *et al.* (1990) except that the base of the manipulator is attached to a motor rather than fixed. Motivated by the ideas for flexible robots in Ge *et al.* (1996, 1998c), two classes of model-free controllers are developed for smart materials robots based on the basic energy–work relationship, which essentially avoid the drawbacks associated with model truncations. Both decentralized and centralized model-free controllers are developed for different control system configurations, and asymptotic stabilities are guaranteed for the damped truncated system of any arbitrary finite number of flexible modes.

The rest of the paper is organized as follows. Smart materials robots are described in § 2. Model-free controllers (both decentralized and centralized) are developed and stability proofs of the closed-loop systems are given in § 3. Numerical simulations are carried out in § 4 to verify the effectiveness of the controllers. Finally, a conclusion is given in § 5.

2. Smart materials robots

We shall consider a smart materials robot with one end of the link rigidly attached to the rotor of a motor and segmented piezoelectric materials covering both sides of the flexible beam as shown in figure 1. The system can be either deployed in space or configured in the horizontal plane. In both cases, the effects of gravity are neglected. As shown in figure 1, there are n pairs of piezoelectric sensors and actuators collocated at n points along the beam. In figure 1, θ_d is the desired joint angular position, v_i is the voltage applied to the ith piezoelectric actuator, τ is the torque applied to the hub, θ is the joint angular position, and $\dot{\theta}$ is the joint angular velocity. Because $\int_0^t I_i \, dt$ defines the electrical charge induced by the ith piezoelectric sensor, which is proportional to the strain, I_i gives the electrical current induced by the ith piezoelectric sensor and is proportional to the change of strain (Won 1995). To facilitate further discussion, define the following vectors

$$\mathbf{I} = [I_1 \quad I_2 \quad \dots \quad I_n]^{\mathrm{T}} \in R^n$$

$$\mathbf{v} = [v_1 \quad v_2 \quad \dots \quad v_n]^{\mathrm{T}} \in R^n$$

For the system under study, there are two kinds of independent controls: the torque control and the voltage controls. The motor is used primarily to move the smart materials robot about the base, and piezoelectric

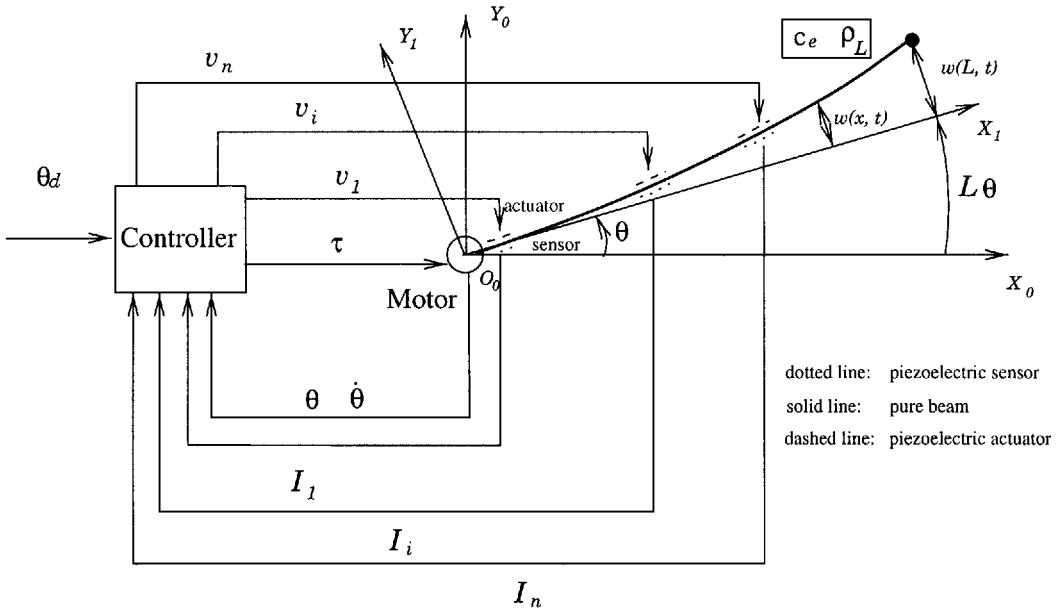

Figure 1. Smart materials robot system.

patches are used to suppress the residual vibration of the robot.

For the system described above, the total work done by external inputs $W = \int_0^t \tau(t)\dot{\theta}(t)\,\mathrm{d}t + \int_0^t \mathbf{v}^{\mathrm{T}}\mathbf{I}\,\mathrm{d}t$, which consists of that done by the torque applied to the hub and that contributed by the voltages applied to the piezoelectric actuators. From the energy–work relationship, i.e. that the increment of the system energy is equal to the work done by external inputs, we have the following equation (Hammond 1981)

$$[E_{\mathrm{k}}(t) + E_{\mathrm{p}}(t)] - [E_{\mathrm{k}}(0) + E_{\mathrm{p}}(0)] = \int_0^t \dot{\theta}(t)\tau(t)\,\mathrm{d}t + \int_0^t \mathbf{I}^{\mathrm{T}}\mathbf{v}\,\mathrm{d}t \quad (1)$$

where $E_{\mathrm{k}}(t)$ and $E_{\mathrm{p}}(t)$ are the total kinetic energy and total potential energy of the system at time t, $E_{\mathrm{k}}(0)$ and $E_{\mathrm{p}}(0)$ are constants representing the kinetic and potential energies at time 0. Therefore, by taking time derivatives of both sides of equation (1), we arrive at

$$\dot{E}_{\mathrm{k}}(t) + \dot{E}_{\mathrm{p}}(t) = \dot{\theta}(t)\tau(t) + \mathbf{I}^{\mathrm{T}}\mathbf{v} \quad (2)$$

which will be used for the controller design in the following section.

3. Model-free controller design

In this section, two classes of model-free controllers are presented by further extending the results in Ge *et al.* (1996, 1998c). The control objective here is to rotate the robot to a desired angular position and simultaneously suppress the residual vibrations effectively. Although the traditional joint PD controller can stabilize flexible robots, the system performance is not very satisfactory because there is no explicit effort introduced to suppress the residual vibrations. The energy-based robust controllers (EBRCs) presented in Ge *et al.* (1996) can achieve the task of regulating the tip with very small residual vibrations, but the resulting performance is very limited because there is only one actuator for each link. In this paper, the ideas of EBRC for flexible robots are extended to smart materials robots for better performance by fully exploiting the fact that more control signals are available.

3.1. *Decentralized model-free controller*

In certain cases, decentralized controllers are very desirable because of (i) the technical difficulties in implementing communications between controllers located at different places; and (ii) the inherent robustness of a decentralized control system.

Consider the following decentralized model-free controller (DMFC)

$$\mathbf{u} = \begin{bmatrix} \tau \\ \mathbf{v} \end{bmatrix} = \begin{bmatrix} -k_{p\theta}[\theta(t) - \theta_{\mathrm{d}}] - k_{v\theta}\dot{\theta}(t) \\ -\mathbf{K}_{ps}\int_0^t \mathbf{I}\,\mathrm{d}t - \mathbf{K}_{vs}\mathbf{I} \end{bmatrix} \quad (3)$$

where $\mathbf{K}_{ps} = \mathrm{diag}\,[k_{ps_i}] \in R^{n\times n}$, $\mathbf{K}_{vs} = \mathrm{diag}\,[k_{vs_i}] \in R^{n\times n}$, and $k_{p\theta}$, $k_{v\theta}$, $k_{vs_i} > 0$, $k_{ps_i} \geq 0$.

It is clear that controller (3) is decentralized in the sense that only local signals are used in constructing the local feedback control. The decentralized nature of the control scheme is also in line with the original objectives of smart materials that sensing and control are done locally for different physical properties. The stability of the system is summarized in the following theorem.

Theorem 1: *DMFC* (3) *can stabilize the smart materials robot system.*

Proof: Consider the following Lyapunov function candidate

$$V_1(t) = E_k(t) + E_p(t) + \tfrac{1}{2}k_{p\theta}[\theta(t) - \theta_{\mathrm{d}}]^2 + \frac{1}{2}\left(\int_0^t \mathbf{I}\,\mathrm{d}t\right)^{\mathrm{T}}\mathbf{K}_{ps}\left(\int_0^t \mathbf{I}\,\mathrm{d}t\right) \quad (4)$$

It is a Lyapunov function candidate because the energy of system $E_k(t) + E_p(t) \geq 0$.

By virtue of equation (2), the time derivative of V_1 is given by

$$\dot{V}_1(t) = \dot{\theta}(t)\tau(t) + \mathbf{I}^{\mathrm{T}}\mathbf{v} + k_{p\theta}[\theta(t) - \theta_d]\dot{\theta}(t) + \mathbf{I}^{\mathrm{T}}\mathbf{K}_{ps}\left(\int_0^t \mathbf{I}\,\mathrm{d}t\right) \quad (5)$$

Substituting the control input (3) into equation (5), we have

$$\dot{V}_1(t) = -k_{v\theta}\dot{\theta}(t)^2 - \mathbf{I}^{\mathrm{T}}\mathbf{K}_{vs}\mathbf{I} \leq 0 \quad (6)$$

Therefore, the closed-loop system is stable in the sense of Lyapunov. □

Remarks:

(1) Although the control scheme is decentralized in nature, it has been shown that it can guarantee the stability of the whole system. In addition, the controller can be easily implemented because of its simplicity.

(2) The decentralized controller is very convenient for the control of a large scale space structure, where communications between different parts of the structure are neither easy to implement nor cost effective, which prevents the actual implementation of a centralized controller.

(3) The decentralized controller is fault tolerant and robust to sensor/actuator failures. For example, if some of the sensors and actuators become faulty, the corresponding local control loops are broken with no input to the system. Further-

more, the overall closed-loop stability is not affected, as can easily be seen from the proof of the theorem.

3.2. *Centralized model-free controller*

In order to further improve the control performance and consider those situations in which centralized controllers can be implemented, we shall study the centralized model-free controller (CMFC) design which fully utilizes the potential of the extra sensing and control capabilities of smart materials robots.

Consider the following CMFC

$$\mathbf{u} = \begin{bmatrix} \tau \\ \mathbf{v} \end{bmatrix} = \begin{bmatrix} -k_{p\theta}[\theta(t) - \theta_{\mathrm{d}}] - k_{v\theta}\dot{\theta}(t) - \tau_{\mathrm{c}} \\ -\mathbf{K}_{ps}\int_0^t \mathbf{I}\,\mathrm{d}t - \mathbf{K}_{vs}\mathbf{I} - \mathbf{v}_{\mathrm{c}} \end{bmatrix} \tag{7}$$

where $\tau_{\mathrm{c}} = \sum_{i=1}^{i=n_0} k_{i\theta} f_{i\theta}(t) \int_0^t \dot{\theta}(s) f_{i\theta}(s)\,\mathrm{d}s$, and $\mathbf{v}_{\mathrm{c}}$ is a column vector defined as

$$\mathbf{v}_c = \begin{bmatrix} \sum_{j=1}^{j=n_1} k_{1j} f_{1j}(t) \int_0^t I_1(s) f_{1j}(s)\,\mathrm{d}s \\ \sum_{j=1}^{j=n_2} k_{2j} f_{2j}(t) \int_0^t I_2(s) f_{2j}(s)\,\mathrm{d}s \\ \vdots \\ \sum_{j=1}^{j=n_n} k_{nj} f_{nj}(t) \int_0^t I_n(s) f_{nj}(s)\,\mathrm{d}s \end{bmatrix} \in R^n$$

$f_{i\theta}, f_{ij}$ are any time integrable signals, $\mathbf{K}_{ps} = \mathrm{diag}\,[k_{ps_i}] \in R^{n\times n}$, $\mathbf{K}_{vs} = \mathrm{diag}\,[k_{vs_i}] \in R^{n\times n}$, $k_{p\theta}$, $k_{v\theta}$, $k_{vs_i} > 0$, $k_{ps_i} \geq 0$, and $k_{i\theta}$, $k_{ij} \geq 0$.

In comparison with the decentralized controller (3), it is the presence of τ_{c} and $\mathbf{v}_{\mathrm{c}}$ that makes (7) a centralized controller, since $f_{i\theta}$ and f_{ij} can be signals from other locations on the link. The closed-loop stability of the system is given below.

Theorem 2: *CMFC* (7) *can stabilize the smart materials robot system.*

Proof: Consider the following Lyapunov function candidate

$$V(t) = V_1(t) + \frac{1}{2}\sum_{i=1}^{i=n_0} k_{i\theta}\left[\int_0^t \dot{\theta}(s) f_{i\theta}(s)\,\mathrm{d}s\right]^2 + \frac{1}{2}\sum_{i=1}^{i=n}\sum_{j=1}^{j=n_i} k_{ij}\left[\int_0^t I_i(s) f_{ij}(s)\,\mathrm{d}s\right]^2 \tag{8}$$

where $V_1(t)$ is defined in equation (4).

Taking the time derivative of V and applying equation (2), we arrive at

$$\begin{aligned}\dot{V}(t) = {} & \tau(t)\dot{\theta}(t) + \sum_{i=1}^{i=n} v_i(t) I_i(t) \\ & + k_{p\theta}[\theta(t) - \theta_d]\dot{\theta}(t) + \sum_{i=1}^{i=n} K_{ps_i}\int_0^t I_i(s)\,\mathrm{d}s I_i(t) \\ & + \sum_{i=1}^{i=n_0} k_{i\theta}\dot{\theta}(t) f_{i\theta}(t)\int_0^t \dot{\theta}(s) f_{i\theta}(s)\,\mathrm{d}s \\ & + \sum_{i=1}^{i=n}\sum_{j=1}^{j=n_i} k_{ij} I_i(t) f_{ij}(t)\int_0^t I_i(s) f_{ij}(s)\,\mathrm{d}s \end{aligned} \tag{9}$$

Substituting (7) into (9) yields

$$\dot{V}(t) = -k_{v\theta}\dot{\theta}(t)^2 - \sum_{i=1}^{i=n} K_{vs_i} I_i^2(t) \leq 0 \tag{10}$$

which means that the closed-loop system is stable in the Lyapunov sense. □

Remarks:

(1) Theoretically, item $\mathbf{K}_{vs}\mathbf{I}$ in controllers (3) and (7) can be replaced by $\mathbf{K}_{vs}\mathbf{p}(\mathbf{I})$, where $\mathbf{p}(\mathbf{I})$ is a column vector with its ith element being the function of I_i. It is found that as long as $p_i(I_i) I_i \geq 0$, $i = 1, \ldots, n$, the stability of the closed loop can be guaranteed. Some examples of $p_i(I_i)$ are listed as follows

$$p_i(I_i) = \begin{cases} I_i \\ \mathrm{sgn}\,(I_i) \\ I_i^3 \end{cases}$$

In the implementation of the controller, according to different system constructions, $p_i(I_i)$ can be selected accordingly.

(2) All the control parameters in controllers (3) and (7) are independent of the system parameters, and thus both controllers are robust to system parameter uncertainties. In fact, the closed-loop systems are stable as long as $k_{p\theta} > 0$, $k_{v\theta} > 0$, $k_{i\theta} \geq 0$, $k_{ps_i} \geq 0$, $k_{vs_i} > 0$, $k_{ij} \geq 0$. Since both the closed-loop stability proofs are independent of the dynamics of the system, drawbacks or problems associated with truncated-model-based approaches are essentially avoided.

(3) For DMFC (3), with the aid of local voltage control, the vibration of the flexible link can be controlled directly and the control performance can be improved. In an attempt to include explicit evaluation of vibration into the controller, non-linear terms τ_{c} and $\mathbf{v}_{\mathrm{c}}$ are introduced into CMFC (7). At this point, we would like to

improve the control performance without destabilizing the system. Theoretically, the stability of the system will not be affected by any time-integrable functions $f_{i\theta}$, f_{ij}, but it is preferable to select $f_{i\theta}, f_{ij}$ to be associated with the vibration of the flexible link. Depending on the actual instrumentation, $f_{i\theta}(t)$, $f_{ij}(t)$ can be chosen as any variable or any combination of variables related to the vibration of the flexible link at any place along the beam. The model-free controllers (3) and (7) constructed here can be easily implemented because $\theta(t)$, $\dot{\theta}(t)$ and $I_i(t)$ are easily obtainable, while $f_{i\theta}$ and f_{ij} can be chosen as any other measurable signals according to different system configurations.

(4) In both Theorems 1 and 2, only closed-loop stability is claimed. It is not easy to prove the asymptotic stability of the system because of the infinite dimensionality of the system. Asymptotic tracking control of an Euler–Bernoulli beam has been achieved in Shifman (1993) under the unrealistic assumption of zero hub inertia. In the following, before giving a rigorous proof based on a truncated model, we shall show that in practice the smart materials robot can only possibly stop at $\theta = \theta_d$ without vibrating, assuming that the link stops at the position $\theta = \theta_1$ (hence $\dot{\theta} = 0$) with $\theta_1 \neq \theta_d$. Due to the existence in practice of internal structural damping in the smart materials robot (structural damping is neglected in the proofs of Theorems 1 and 2), the link must tend to stop vibrating and finally be static at the undeformed position. Recalling that I_i is proportional to the change of strain, we have $\mathbf{I} = \mathbf{0}$. Hence there is no energy input to the system since $\dot{\theta}\tau + \mathbf{I}^T\mathbf{v} = 0$ and the robot under study is in the horizontal plane. Furthermore, $\int_0^t I_i \, dt$ is proportional to the strain, $\int_0^t \mathbf{I} \, dt = \mathbf{0}$ when the link is undeformed, as signals $f_{i\theta}, f_{ij}$ are chosen to be zero when the link is at rest because these functions are associated with the vibrations of the link. Consequently, except that the first term in τ is not equal to zero, other terms in τ are equal to zero and $\mathbf{v} = \mathbf{0}$. Therefore, τ is a non-zero constant and thus $\theta = \theta_1$ cannot hold. The only possibility is that $\theta = \theta_d$, which implies that tip regulation can be achieved in practice.

Theorem 3: *Controller* (3) *can guarantee the asymptotic stability of a damped truncated system where the flexible deflection is described by arbitrarily any finite number of flexible modes. Furthermore, controller* (7) *can also guarantee the asymptotic stability of the same truncated system if* $f_{i\theta}$, f_{ij} *are selected as functions that are equal to zero when the flexible smart materials robot is undeformed.*

The proof is very much the same as in Ge *et al.* (1998b). It is given here for completeness and easy reference.

Proof: Using the same Lyapunov functions (4) and (8), we consider the motion of the system in the largest invariant set in the set $\dot{V}_1 = 0$ ($\dot{V} = 0$). In both cases, we have $\dot{\theta} \equiv 0$ and $\mathbf{I} \equiv \mathbf{0}$. Subsequently, $\ddot{\theta} = 0$, $\tau = -k_{p\theta}(\theta - \theta_d)$. Furthermore, according to Remark (4), $\mathbf{v} = \mathbf{0}$.

With the aid of the notable Hamilton's principle, considering the motion of system in $\dot{V}_1 = 0$ ($\dot{V} = 0$), we have the following PDEs and boundary conditions (BCs) of the system (Ge *et al.* 1998b)

$$c_e \frac{\partial w^2(0,t)}{\partial x^2} - k_{p\theta}(\theta - \theta_d) = 0 \tag{11}$$

$$\rho_L \ddot{w}(x,t)] = -c_e \frac{\partial^4 w(x,t)}{\partial x^4} \tag{12}$$

$$w(0,t) = 0, \frac{\partial w(0,t)}{\partial x} = 0, \frac{\partial^2 w(0,t)}{\partial x^2} = 0 \tag{13}$$

$$c_e \frac{\partial^3 w(L,t)}{\partial x^3} = m_3 \ddot{w}(L,t) \tag{14}$$

where $w(x,t)$ is the deflection of the link, c_e is the electromechanical stiffness per length of the smart materials beam, and m_3 is the mass of the tip payload.

Using the method of separating variables (Meirovitch 1986), the solution to (12) is assumed to be of the form $w(x,t) = \Psi(x)Q(t)$, and equation (12) becomes

$$\frac{\Psi''''(x)}{\Psi(x)} \cdot \frac{c_e}{\rho_L} = -\frac{\ddot{Q}(t)}{Q(t)} \tag{15}$$

where primes denote the derivatives of x and dots denote the derivatives of t. It is clear that the left hand side of equation (15) is a pure function of x whereas the right-hand side depends on t only. Therefore, both sides of (15) should be equal to a constant. If k is used to denote the constant, the PDE (15) can be reduced into two ordinary differential equations (ODEs), namely

$$\ddot{Q}(t) = -kQ(t) \tag{16}$$

and

$$\Psi''''(x) = \frac{\rho_L}{c_e} k \Psi(x) \tag{17}$$

The BCs become

$$\left.\begin{aligned}\Psi(0) &= 0\\ \Psi'(0) &= 0\\ \Psi''(L) &= 0\\ \Psi'''(L) &= -\frac{m_3}{c_e}k\Psi(L)\end{aligned}\right\} \tag{18}$$

We will consider equation (17) and conditions (18) with regard to different values of the constant k.

It can be proved that when $k < 0$ or $k = 0$, the solution to equation (17) is trivial. Then we just need to consider the case for $k > 0$.

Letting $k > 0$, (17) can be rewritten as

$$\Psi''''(x) = \left(\frac{\nu}{L}\right)^4 \Psi(x) \tag{19}$$

with

$$\left(\frac{\nu}{L}\right)^4 = k\frac{\rho_L}{c_e} \tag{20}$$

The general solution to (19) is of the form

$$\Psi(x) = C_1\cos\frac{\nu x}{L} + C_2\cosh\frac{\nu x}{L} + C_3\sin\frac{\nu x}{L} + C_4\sinh\frac{\nu x}{L} \tag{21}$$

From BCs (18), a set of equations is obtained

$$\left.\begin{aligned} C_1 + C_2 &= 0\\ C_3 + C_4 &= 0\\ -C_1\cos\nu + C_2\cosh\nu - C_3\sin\nu - C_4\sinh\nu &= 0\\ C_1\left(\sin\nu + \frac{m_3\nu}{\rho_L L}\cos\nu\right) + C_2\left(\sinh\nu + \frac{m_3\nu}{\rho_L L}\cosh\nu\right)\cosh\nu &\\ + C_3\left(\frac{m_3\nu}{\rho_L L}\sin\nu - \cos\nu\right) + C_4\left(\cosh\nu + \frac{m_3\nu}{\rho_L L}\sinh\nu\right) &= 0\end{aligned}\right\} \tag{22}$$

To obtain non-trivial solutions, the determinant of the coefficient matrix of equations (22) must be zero, i.e.

$$1 + \cosh\nu\cos\nu + \frac{m_3\nu}{\rho_L L}(\sinh\nu\cos\nu - \cosh\nu\sin\nu) = 0 \tag{23}$$

which may be satisfied by an infinite number of ν. Note that only positive ν are used.

Considering the first three equations in (22), the general solution of (21) is

$$\Psi(x) = C_2\left[\cosh\frac{\nu x}{L} - \cos\frac{\nu x}{L} - \gamma\left(\sinh\frac{\nu x}{L} - \sin\frac{\nu x}{L}\right)\right] \tag{24}$$

where

$$\gamma = \frac{\cosh\nu + \cos\nu}{\sinh\nu + \sin\nu} \tag{25}$$

Letting $0 < \nu_1 < \nu_2 < \cdots < \infty$ be an infinite number of positive solutions to equation (23), an infinite number of solutions to the boundary value problem can be given by

$$\begin{aligned}\psi_i(x) &= A_i\left[\cosh\frac{\nu_i x}{L} - \cos\frac{\nu_i x}{L} - \gamma_i\left(\sinh\frac{\nu_i x}{L} - \sin\frac{\nu_i x}{L}\right)\right]\\ &= A_i\bar{\psi}_i(x), \qquad i = 1,2,\ldots\end{aligned} \tag{26}$$

where γ_i is calculated by equation (25) with corresponding ν_i, and constants A_i are to be determined later.

Letting $k = \omega^2$, with ω being a non-zero number, equation (16) can be rewritten as

$$\ddot{Q}(t) + \omega^2 Q(t) = 0 \tag{27}$$

which indicates that $Q(t)$ is harmonic with frequency ω. Corresponding to the infinite number of ν_i, an infinite number of natural frequencies

$$\omega_i = \frac{\nu_i^2}{L^2}\sqrt{\frac{c_e}{\rho_L}} \tag{28}$$

exist. Subsequently, an infinite number of solutions to equation (27) can be obtained

$$q_i(t) = B_i\cos\omega_i t + C_i\sin\omega_i t \tag{29}$$

where B_i and C_i are constants that will be determined later from the initial conditions. Note that equation (12) is linear and homogeneous; from the superposition or linearity principle (Meirovitch 1986), a solution $w(x,t)$ can be given as

$$w(x,t) = \sum_{i=1}^{\infty}\psi_i(x)q_i(t) \tag{30}$$

The remaining problem is to determine A_i, B_i and C_i. We introduce the following orthogonal conditions

$$\rho_L\int_0^L \psi_i\psi_j\,\mathrm{d}x + m_3\psi_i(L)\psi_j(L) = \begin{cases}0 & i \neq j\\ \rho_L & i = j\end{cases} \tag{31}$$

$$c_e\int_0^L \psi_i''\psi_j''\,\mathrm{d}x = \begin{cases}0 & i \neq j\\ \omega_i^2\rho_L & i = j\end{cases} \tag{32}$$

Let $w_0(x,t_0)$ and $\dot{w}_0(x,t_0)$ denote the 'initial' deflection and velocity profiles of the flexible link. We have

$$w_0(x,t_0) = \sum_{i=0}^{i=\infty}\psi_i(x)(B_i\cos\omega_i t_0 + D_i\sin\omega_i t_0) \tag{33}$$

$$\dot{w}_0(x,t_0) = \sum_{i=0}^{i=\infty}\psi_i(x)(-B_i\sin\omega_i t_0 + D_i\cos\omega_i t_0)\omega_i \tag{34}$$

Note that the 'initial' moment t_0 should denote the moment when the system motion enters the invariant set, rather than the initial operating moment, since we are considering the motion of the system in the largest invariant set in the set $\dot{V} = 0$.

Define

$$\eta_{i1} = \int_0^L w_0(x,t_0)\psi_i(x)\,\mathrm{d}x + \frac{m_3}{\rho_L}w_0(L,t_0)\psi_i(L) \tag{35}$$

$$\eta_{i2} = \frac{1}{\omega_i}\left[\int_0^L \dot{w}_0(x,t_0)\psi_i(x)\,\mathrm{d}x + \frac{m_3}{\rho_L}w\dot{w}_0(L,t_0)\psi_i(L)\right] \tag{36}$$

From the expansion theorem (Meirovitch 1986), it can be seen that the infinite summation in equation (30) is

absolutely and uniformly convergent. It implies that if equations (33) and (34) are substituted into η_{i1} and η_{i2}, the corresponding integrals can be calculated by terms, i.e.

$$\eta_{i1} = \sum_{j=0}^{j=\infty} (B_j \cos \omega_j t_0 + D_j \sin \omega_j t_0) \times \left[\int_0^L \psi_j(x)\psi_i(x)\,\mathrm{d}x + \frac{m_3}{\rho_L}\psi_j(L)\psi_i(L) \right] \quad (37)$$

$$\eta_{i2} = \sum_{j=0}^{j=\infty} \frac{\omega_j}{\omega_i} (-B_j \sin \omega_j t_0 + D_j \cos \omega_j t_0) \times \left[\int_0^L \psi_j(x)\psi_i(x)\,\mathrm{d}x + \frac{m_3}{\rho_L}\psi_j(L)\psi_i(L) \right] \quad (38)$$

Invoking the orthogonal condition (31), we arrive at

$$\eta_{i1} = B_i \cos \omega_i t_0 + D_i \sin \omega_i t_0$$
$$\eta_{i2} = -B_i \sin \omega_i t_0 + D_i \cos \omega_i t_0$$

Then B_i and D_i can be determined by

$$B_i = \eta_{i1} \cos \omega_i t_0 - \eta_{i2} \sin \omega_i t_0$$
$$D_i = \eta_{i1} \sin \omega_i t_0 + \eta_{i2} \cos \omega_i t_0$$

Furthermore, by using orthogonal conditions (31) and (32), it is found that (Ge *et al.* 1998b)

$$A_i = \left[\frac{1}{\int_0^L \bar{\psi}_i^{\,2}(x)\,\mathrm{d}x + \frac{m_3}{\rho_L}\bar{\psi}_i^{\,2}(L)} \right]^{1/2} \quad (39)$$

From modal analysis, those modes with comparatively low frequencies are dominant; we have the following reasonable approximation

$$w(x,t) = \sum_{i=1}^{i=N} \psi_i(x) q_i(t) \quad (40)$$

where N is the number of flexible modes used to approximate the deflection. Substituting (40) into (11) yields

$$\sum_{i=0}^{i=N} a_i q_i(t) = 0 \quad (41)$$

where

$$a_0 = 1, q_0 = k_{p\theta}(\theta - \theta_\mathrm{d}), a_i = c_e \psi''(0) = 2\frac{A_i \nu_i^2}{L^2} \neq 0$$

For the summation in (41), it is easy to find the following inner product

$$\langle q_i, q_j \rangle := \lim_{T\to\infty} \int_0^\mathrm{T} q_i(t) q_j(t)\,\mathrm{d}t \begin{cases} = 0, & i \neq j \\ \neq 0, & i = j \end{cases} \quad (42)$$

Applying this inner product to the summation (41) leads to the fact that each q_i $(i = 0, 1, \ldots, N)$ must be zero, and subsequently $\theta = \theta_\mathrm{d}$ and $w(x,t) = 0$. It implies that the truncated system is at the largest invariant set in the set $\dot{V}_1 = 0$ ($\dot{V} = 0$).

Invoking LaSalle's theorem, the joint angle θ and the N flexible modes of the truncated system are asymptotically stable with respect to the final position. □

4. Numerical simulation

In this section, we shall investigate the performance of both DMFC and CMFC presented in this paper in comparison with the traditional joint PD controller and the EBRC in Ge *et al.* (1996). The system parameters are given in table 1. The system is simulated by an assumed modes method (AMM) model in which the first four modes' shape functions are considered. A fourth-order Runge–Kutta program with adaptive-step-size is used to

Parameter	Symbol (unit)	Value
pure beam thickness	a (m)	0.008
piezoelectric actuator thickness	c_1 (m)	0.0008
piezoelectric sensor thickness	c_2 (m)	0.0004
width of the beam	b (m)	0.01
length of the piezoelectric material	l (m)	0.01
length of the beam	L (m)	1
density of the pure beam	ρ_1 (kg/m^3)	500
density of the piezoelectric material	ρ_2 (kg/m^3)	100
moment of inertia of the hub	I_h (kg/m^2)	3.0
tip payload	m_3 (kg)	0.001
stiffness of the beam	c_{11}^m (N/m^2)	6×10^8
stiffness of the piezoelectric material	c_{11}^s (N/m^2)	8×10^6
permeability of the piezoelectric material	μ_{33} (H/m)	1.2×10^{-6}
coupling parameter	h_{12} (v/m)	5×10^{11}
impermittivity	β_{22} (m/F)	4×10^{14}

Table 1. System parameters.

solve the ODEs numerically (Ge *et al.* 1998a). The sampling interval is set to be 0.005 s. For simplicity, only one pair of piezoelectric actuator and sensor is used in the simulation because it is enough to show the effectiveness of the model-free controllers. The pair of piezoelectric patches is located at $x = 0.1L$ of the beam, L being the full length of the link. The initial and final desired positions of the smart materials robot are $\theta(0) = 0^\circ$ and $\theta_d = 60^\circ$. The robot is assumed to be initially at rest without any deformation.

In order to compare the model-free controllers with the traditional joint PD controller, we shall firstly consider the closed-loop performance under the pure joint PD controller

$$\tau(t) = -k_{p\theta}[\theta(t) - \theta_d] - k_{v\theta}\dot{\theta} \tag{43}$$

while the voltage control is set to zero, which means that no explicit efforts are made on the residual vibration suppression. However, different $k_{p\theta}$ and $k_{v\theta}$ will lead to different system performance. By taking the smart materials robot as a rigid one, $k_{p\theta}$ and $k_{v\theta}$ are selected to make the closed loop critically damped. The corresponding rigid motion error equation of the smart materials robot is

$$m_e\ddot{e}(t) + k_{v\theta}\dot{e}(t) + k_{p\theta}e(t) = 0 \tag{44}$$

where $e(t) = \theta(t) - \theta_d$, $\dot{e}(t) = \dot{\theta}(t)$ and $\ddot{e}(t) = \ddot{\theta}(t)$ since θ_d is constant, the equivalent inertia of the joint

$$m_e = I_h + \tfrac{1}{3}ab\rho_1 L^2 + \int_{0.1L}^{0.1L+l}(c_1 + c_2)b\rho_2 x^2\,dx + m_3L^2 = 3.0143\ \text{kg m}^2 \tag{45}$$

where $\frac{1}{3}ab\rho_1L^2$, $\int_{0.1L}^{0.1L+l}(c_1 + c_2)b\rho_2x^2\,dx$ and m_3L^2 are respectively the moments of inertia of the robot, the piezoelectric patches and the tip payload with respect to the base, and parameters I_h, a, b, c_1, c_2, ρ_1, ρ_2, m_3, L, l are defined in table 1.

To avoid possible overshoot of the angular position, assume that the equivalent system is lightly overdamped with a damping factor of $\xi = 1.0195$. The resulting $k_{v\theta}$ and $k_{p\theta}$ are as follows

$$\left.\begin{aligned} k_{v\theta} &= 2m_e\xi\omega \\ k_{p\theta} &= m_e\omega^2 \end{aligned}\right\} \tag{46}$$

where ω is the natural frequency of the 2nd-order system (44). Letting $\omega = 2.5487$, we have $k_{p\theta} = 19.5813$ and $k_{v\theta} = 15.6650$, which are used for the pure joint PD controller and the controllers listed below.

The energy-based robust controller in Ge *et al.* (1996) is given by

EBRC:

$$\tau(t) = -k_{p\theta}[\theta(t) - \theta_d] - k_{v\theta}\dot{\theta} - k_{1\theta}w(L,t) \times \int_0^t \dot{\theta}(\xi)w(L,\xi)\,d\xi \tag{47}$$

where $w(L,t)$ is the tip deflection of the robot.

The decentralized and centralized model-free controllers to be compared with are given by

DMFC:

$$\mathbf{u} = \begin{bmatrix} \tau \\ v_1 \end{bmatrix} = \begin{bmatrix} -k_{p\theta}[\theta(t) - \theta_d] - k_{v\theta}\dot{\theta}(t) \\ -k_{vs_1}I_1(t) \end{bmatrix} \tag{48}$$

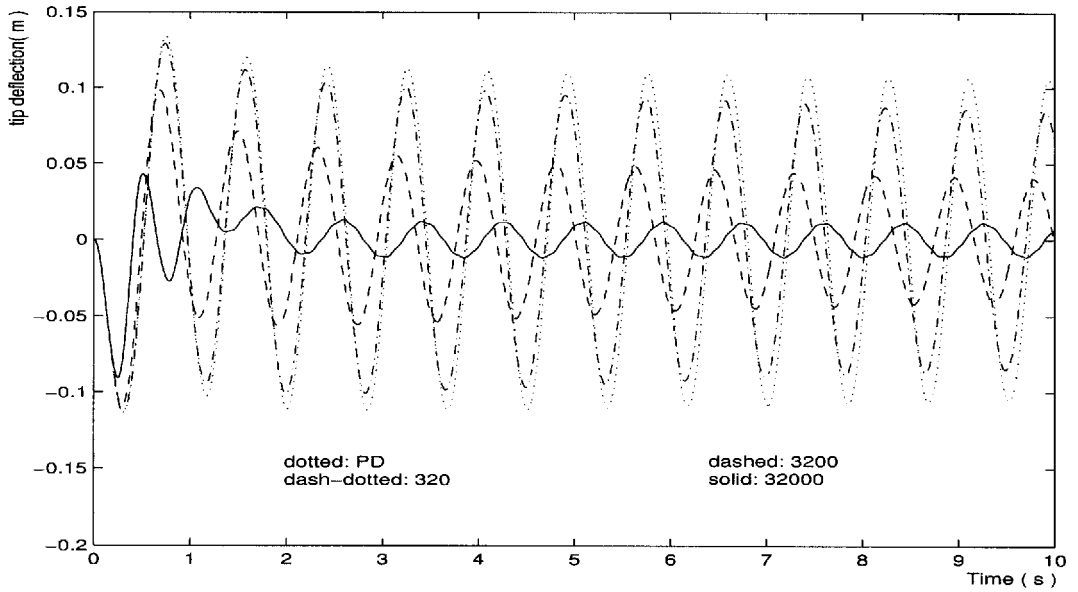

Figure 2. Tip deflections of EBRC with different $k_{1\theta}$s.

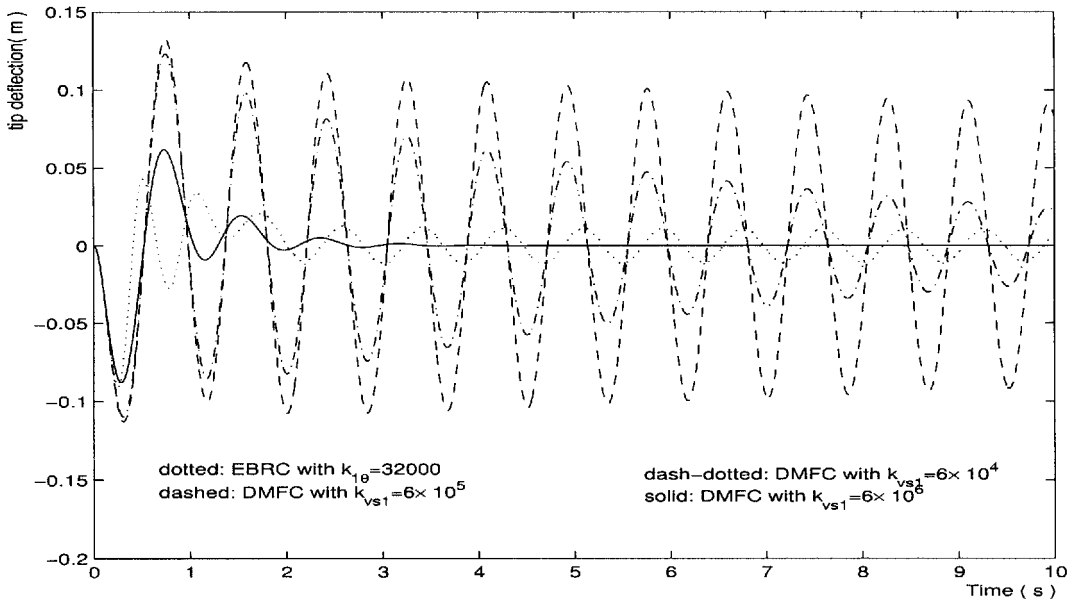

Figure 3. Tip deflections: EBRC versus DMFC.

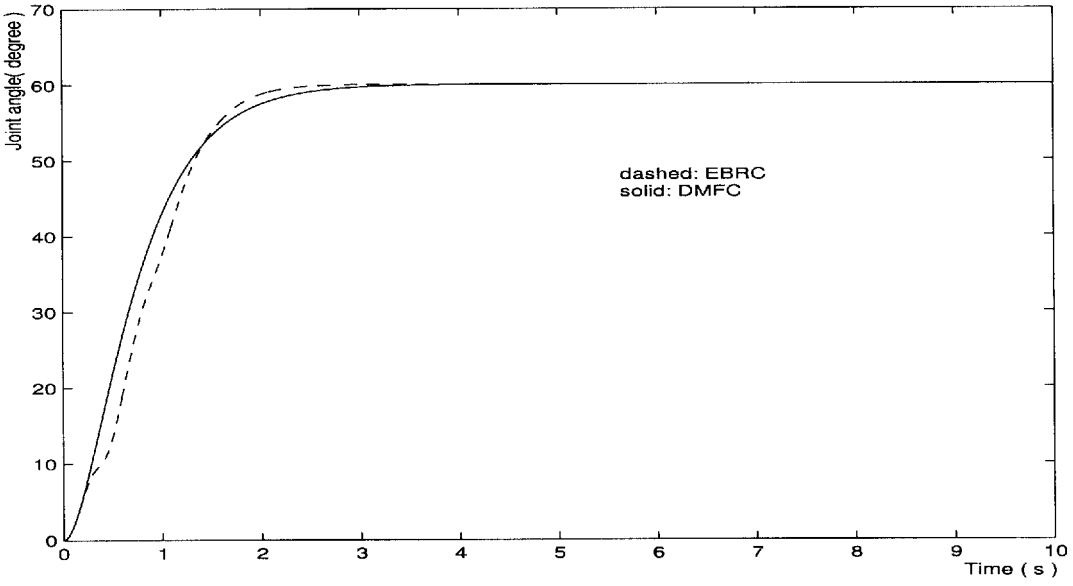

Figure 4. Joint angles: EBRC versus DMFC.

CMFC:

$$\mathbf{u} = \begin{bmatrix} \tau \\ v_1 \end{bmatrix} = \begin{bmatrix} -k_{p\theta}[\theta(t) - \theta_d] - k_{v\theta}\dot{\theta}(t) - k_{1\theta} w(L,t) \int_0^t \dot{\theta}(\xi) w(L,\xi)\, d\xi \\ -k_{vs_1} I_1(t) \end{bmatrix} \tag{49}$$

4.1. *PD control versus EBRC*

Figure 2 shows the tip deflections of PD control and EBRC with different $k_{1\theta}$s. It can be seen that PD control gives the worst performance whereas EBRC can suppress the residual vibration effectively as $k_{1\theta}$ increases. It can be seen that when $k_{1\theta}$ is small ($k_{1\theta} = 320$), the residual vibration cannot be effectively suppressed, but it can be suppressed really quickly when $k_{1\theta}$ is large enough, say $k_{1\theta} = 32\,000$. However, in practice, measurement noise does exist, feedback gain cannot be set arbitrarily large which actually limits the effectiveness of the EBRC scheme. On the other hand, we will show that CMFC can achieve comparatively good performance with lower feedback gain, say $k_{1\theta} = 320$, in §4.3.

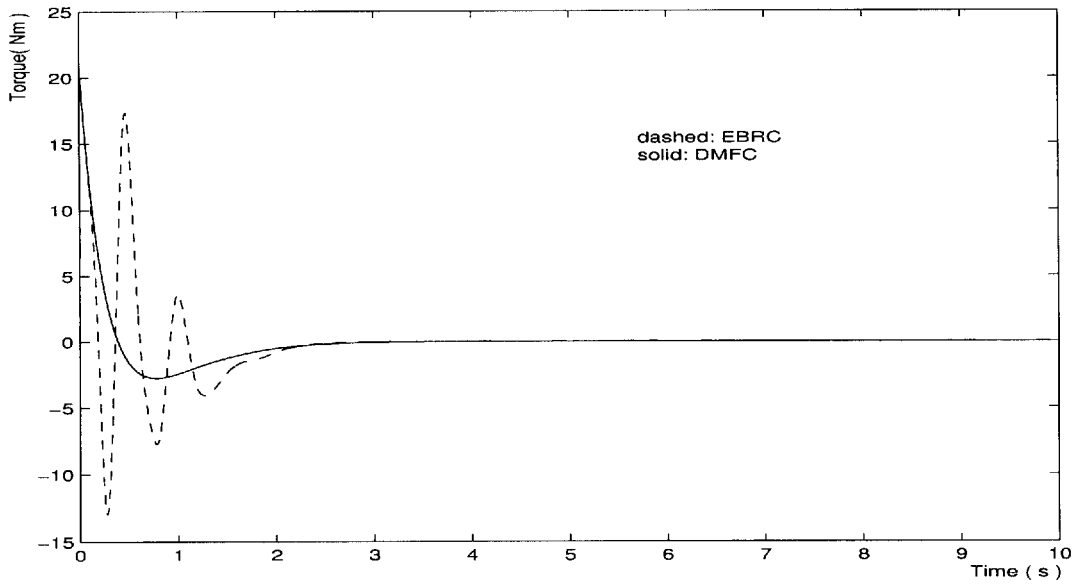

Figure 5. Variations of torque control: EBRC versus DMFC.

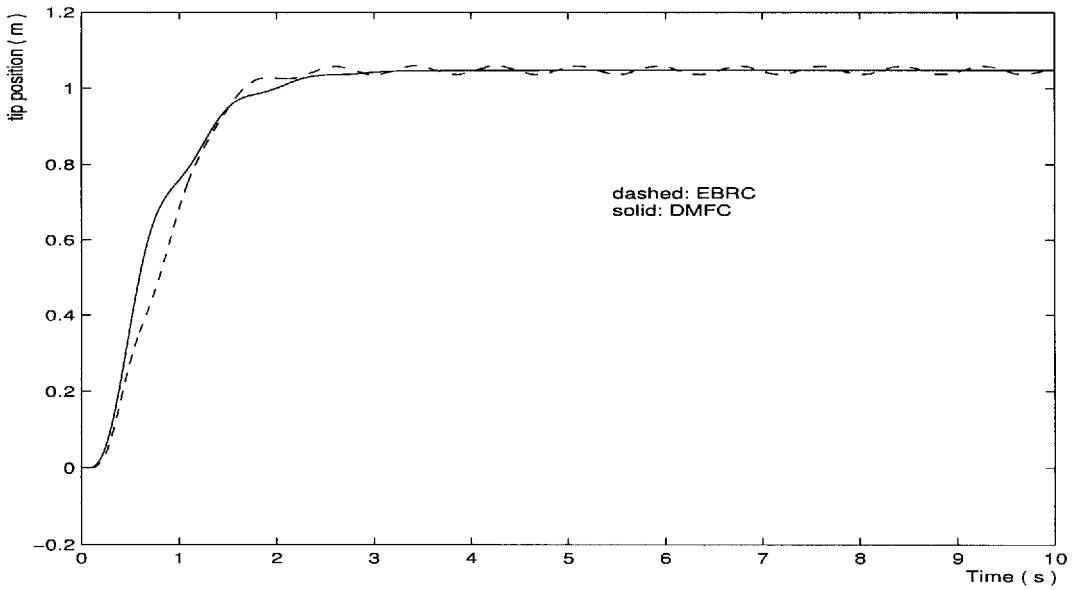

Figure 6. Tip positions: EBRC versus DMFC.

4.2. *EBRC versus DMFC*

Figure 3 shows the tip deflections of DMFC with different feedback gains ($k_{vs1} = 6 \times 10^4$, 6×10^5 and 6×10^6) in comparison with the relatively good EBRC with gain $k_{1\theta} = 32\,000$. It can be seen from figure 3 that when the feedback gain k_{vs1} is large enough, DMFC is much more effective than EBRC in suppressing residual vibration. For both DMFC with $k_{vs1} = 6 \times 10^6$ and EBRC with $k_{1\theta} = 32\,000$, although the transient responses are about the same, there is a big difference at steady state. While there is no residual vibration at steady state for DMFC, there is residual vibration of small magnitude for EBRC.

For better understanding, and a clear presentation, other signals in the closed-loop are compared between EBRC and DMFC with $k_{vs1} = 6 \times 10^6$. Figure 4 shows the bounded joint angle responses of the corresponding EBRC and DMFC. Though not much conclusion can be made from the joint angle responses, the torque control of DMFC is much smoother and of smaller magnitude during the transient period than that of EBRC, as shown in figure 5.

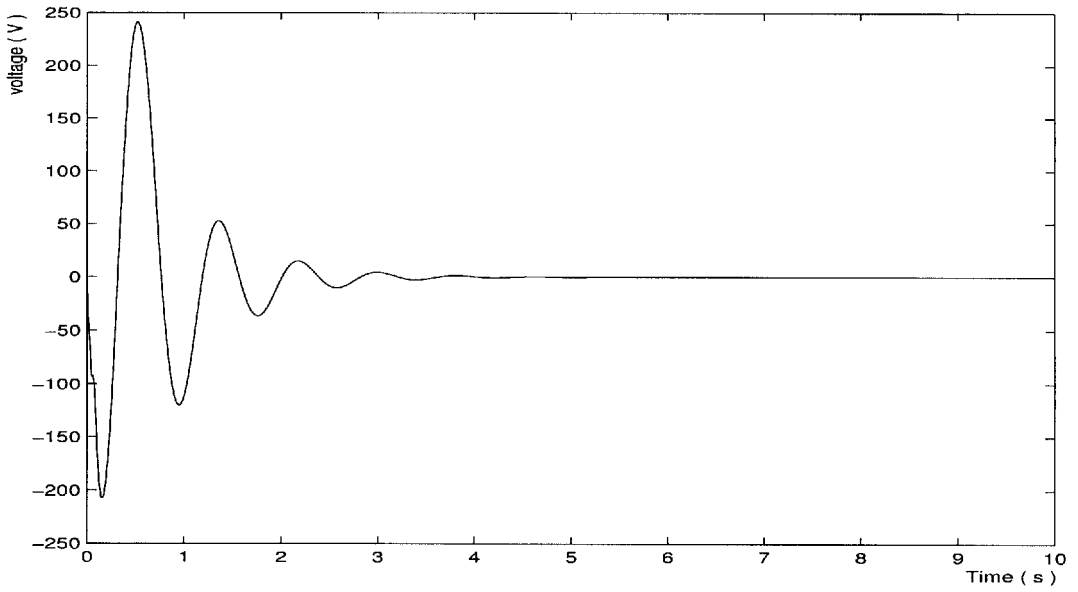

Figure 7. Voltage input of DMFC.

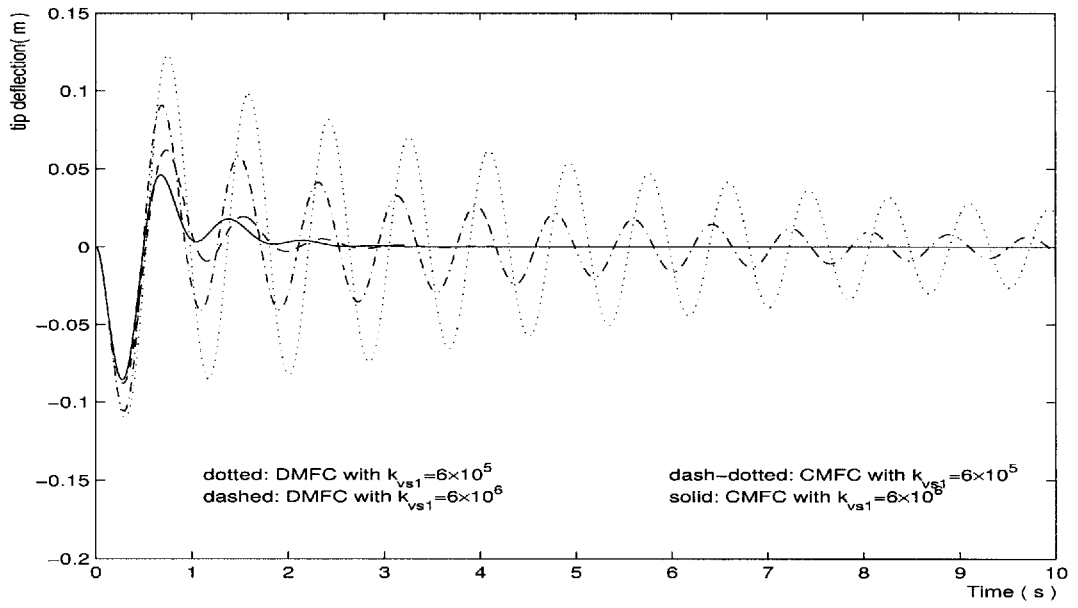

Figure 8. Tip deflections: DMFC versus CMFC.

What we care about most is the trajectory of the tip. The tip is required to converge fast with as small residual vibration or overshoot as possible to improve positioning accuracy. Under the assumption of small deflection, the tip position of the robot can be approximated by

$$p_t = L\theta(t) + w(L,t) \tag{50}$$

where p_t is the tip position, $w(L,t)$ is the tip deflection of the smart materials robot and the angular position is represented in radians instead of degrees. The tip positions under different controllers are depicted in figure 6. It can be seen that the tip position of the DMFC can converge faster and smoother than that of the EBRC. There is hardly any vibration in tip position for the DMFC. This is very desirable in trajectory control.

For completeness, the voltage acting on the piezoelectric actuator in DMFC is shown in figure 7. It can be seen that the voltage control signal is also bounded.

4.3. *DMFC versus CMFC*

Figure 8 shows the tip deflections of DMFC and CMFC with different voltage feedback gains

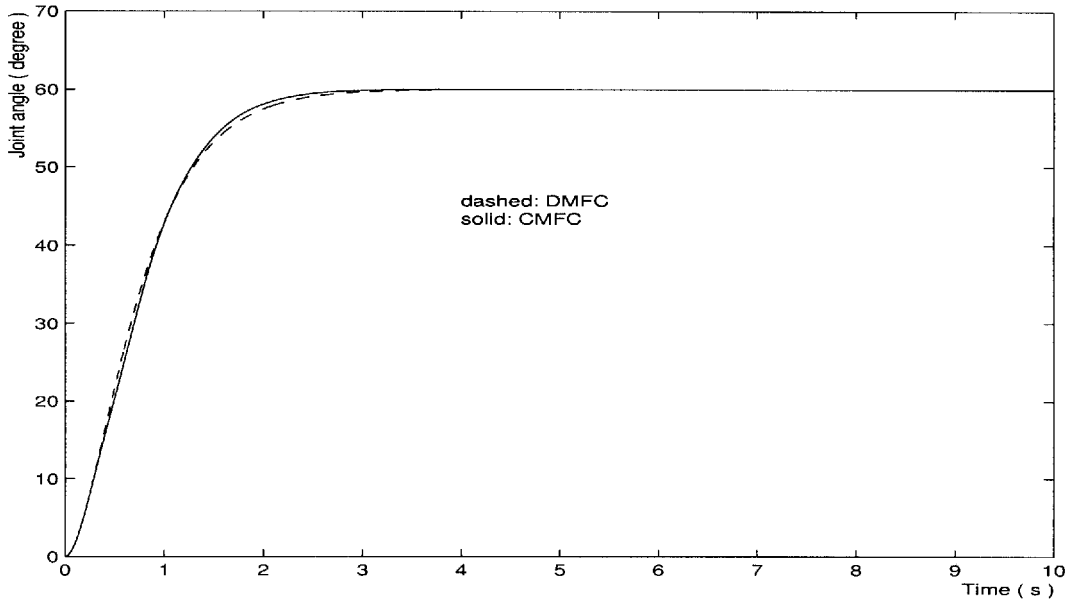

Figure 9. Joint angle variations: DMFC versus CMFC.

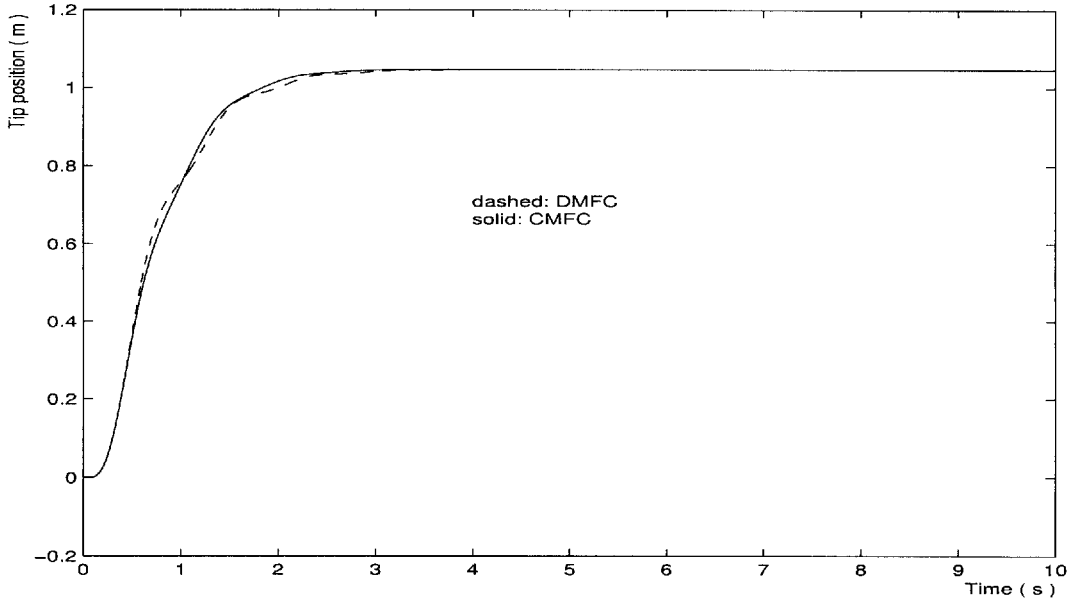

Figure 10. Tip positions: DMFC versus CMFC.

$k_{vs1} = 6 \times 10^5$ and 6×10^6. It can be seen that the performance of CMFC is better than that of DMFC in suppressing residual vibration for the same feedback gain.

For completeness and clarity in presentation, other signals in the closed loop for DMFC and the CMFC with $k_{vs1} = 6 \times 10^6$ are included. Figures 9 and 10 show the joint angle responses and tip positions respectively, while figures 11 and 12 give the torque control and voltage control respectively. It can be seen that all the closed-loop signals are bounded.

If more precise control performance is required, more pairs of piezoelectric actuators and sensors can be bonded and appropriate $f_{i\theta}$s and f_{ij}s can be chosen to improve the performance. DMFC and CMFC can be applied according to different system configurations. When properly constructed, both of them can achieve good control performance. Through the simulation study, it can be seen that both DMFC and CMFC are very effective in controlling residual vibration despite their low authority in control action.

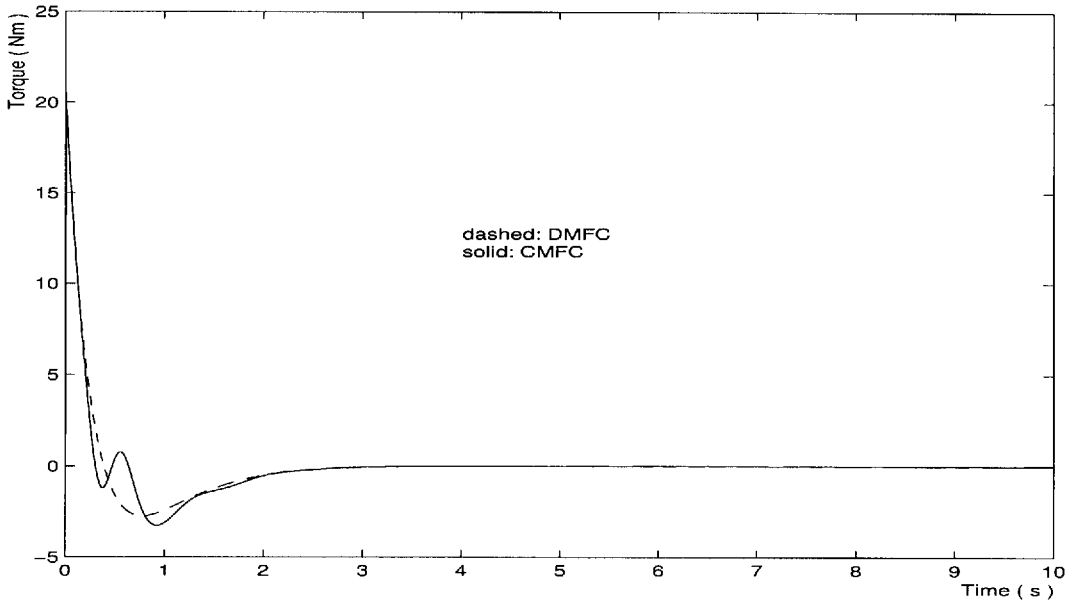

Figure 11. Variation of torque control: DMFC versus CMFC.

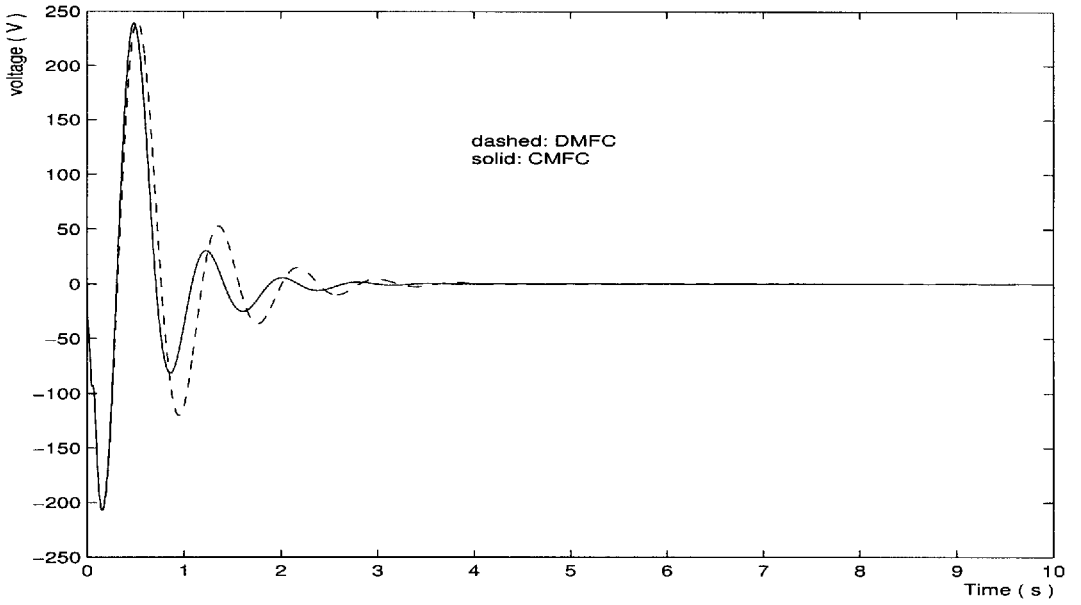

Figure 12. Variation of voltage signal: DMFC versus CMFC.

5. Conclusion

In this paper, two kinds of model-free controllers have been investigated on the basis of the basic energy–work relationship without the need to know the dynamics of the system. Both of them can stabilize the closed-loop system, and asymptotic stability can be guaranteed for the damped system with arbitrarily any finite number of flexible modes. The controllers can be easily implemented because the signals used in the feedback control can be measured directly or be chosen as measurable ones. It has been verified that the controllers can suppress the residual vibrations of the robot more effectively than the traditional joint PD controller and EBRCs through numerical simulation.

References

AOUSTIN, Y., CHEVALLEREAU, C., GLUMINEAU, A., and MOOG, C. H., 1994, Experimental results for the end-effector control of a single flexible robotic arm. *IEEE Transactions on Control Systems Technology*, **2**. 371–381.

BAILY, T., and HUBBARD, J. E., 1985, Distributed piezoelectric-polymer active vibration control of a cantilever beam. *Journal of Guidance, Control, and Dynamics*, **8**, 605–611.

CRAWLEY, E. F., and LUIS, J. 1987, Use of piezoelectric actuators as elements of intelligent structures. *AIAA Journal*, **25**, 1373–1385.

CUNDARI, M., and ABEDIAN, B., 1991, The dynamic behavior of a polyvinylidene fluoride piezoelectric motional device. In G. K. Haritos and A. V. Srinavasan (eds) *Smart Structures and Materials*, Vol. 24 (New York: American Society of Mechanical Engineers), pp. 25–31.

GE, S. S., LEE, T. H., and HARRIS, C. J., 1998a, *Adaptive Neural Network Control of Robot Manipulators* (River Edge, NJ: World Scientific).

GE, S. S., LEE, T. H., and ZHU, G., 1996, Energy-based robust controller design for multi-link flexible robots. *Mechatronics*, **6**, 779–798.

GE, S. S., LEE, T. H., and ZHU, G., 1998b, Asymptotically stable end-point regulation of a flexible scara/cartesian robot. *IEEE/ASME Transactions on Mechatronics*, **3**, 138–144.

GE, S. S., LEE, T. H., and ZHU, G., 1998c, Improving regulation of a single-link flexible manipulator with strain feedback. *IEEE Transactions on Robotics and Automation*, **14**, 179–185.

HAMMOND, P., 1981, *Energy Methods in Electromagnetism* (Oxford: Clarenden Press).

LANARI, L., and WEN, J. T., 1992, Aymptotically stable set point control laws for flexible robots. *Systems and Control Letters*, **19**, 119–129.

MEIROVITCH, L., 1986, *Elements of Vibration Analysis* (New York: McGraw-Hill).

SHIFMAN, J. J., 1993, Lyapunov functions and the control of the Euler-Bernoulli beam. *International Journal of Control*, **57**, 971–990.

SICILIANO, B., and BOOK, W. J., 1988, A singular perturbation approach to control lightweight flexible manipulators. *International Journal of Robotics Research*, **7**, 79–90.

VARADAN, V. K., HONG, S. Y., and VARADAN, V. V., 1990, Piezoelectric sensors and actuators for active vibration damping using digitial control. In: *IEEE Ultrasonics Symposium*, Honolulu, HI, pp. 1211–1214.

VUKOVICH, G., and YOUSEFI-KOMA, A., 1996, A non-collocated active traveling wave control of smart structures using distributed transducers. In: *Proceedings of the 1996 IEEE International Conference on Control Applications*, Dearborn, MI, pp. 297–302.

WON, C. C., 1995, Piezoelectric transformer. *Journal of Guidance, Control, and Dynamics*, **18**, 96–101.

YANG, S. M., and LEE, Y. J., 1994, Interaction of structure vibration and piezoelectric actuation. *Smart Materials and Structures*, **3**, 494–500.

ZHU, G., LEE, T. H., and GE, S. S., 1997, Tracking control of a single-link flexible robot: A backstepping approach. *Dynamics and Control*, **7**, 341–360.